Distributed quantum information processing via single atom driving

Jing-Xin Liu[1], Jun-Yao Ye[1], Lei-Lei Yan[1], Shi-Lei Su[1,3] and **Mang Feng[1,2]**

[1] School of Physics, Zhengzhou University, Zhengzhou 450001, People's Republic of China
[2] State Key Laboratory of Magnetic Resonance and Atomic and Molecular Physics, Wuhan Institute of Physics and Mathematics, Chinese Academy of Sciences, Wuhan 430071, People's Republic of China

E-mail: slsu@zzu.edu.cn and mangfeng@wipm.ac.cn

Abstract

We propose an unconventional scheme for quantum entangled state distribution (QESD) and quantum state transfer (QST) based on a fiber–cavity–atom system, in which three atoms are confined, respectively, in three bimodal cavities connected with each other by optical fibers. The key feature of the scheme is the virtual excitation of photons, which yields QESD and QST between the two atoms in the edge cavities conditioned on one-step operation only on the atom in the middle cavity. No actual operation is performed on the two atoms in the edge cavities throughout the scheme. Robustness of the scheme to operational imperfection and dissipation is discussed and the results show that system fidelity is mostly above 95%. Finally, the experimental feasibility is justified using laboratory-available values.

Keywords: distributed quantum information processing, quantum network, quantum state transfer

(Some figures may appear in colour only in the online journal)

1. Introduction

Quantum entangled state distribution (QESD), which aims to achieve quantum entanglement between distant nodes in a quantum network [1–3], plays a critical role in quantum cryptography implementation [4, 5], quantum secret sharing [6], quantum teleportation [7] and distributed quantum computation [8]. So far, there have been many schemes proposed for QESD using single atoms [2, 9, 10], trapped ions [3, 11], atomic ensembles [12] and nitrogen-vacancy centers [13], as well as cavity quantum electrodynamics [14–25]. Furthermore, QESD in noisy channels [26, 27], even over long distances [28], has also been well studied in photonic systems. Fast QESD with atomic ensembles and fluorescent detection has also been studied [29]. Quantum state transfer (QST) [1, 30] aims to transmit quantum states (or quantum information) from one node to another in a quantum network. The mathematical form of the simplest QST between two nodes A and B can be expressed as $|\psi\rangle_A |0\rangle_B \rightarrow |0\rangle_A |\psi\rangle_B$, where $|\psi\rangle$ is the transferred state. Like QESD, a lot of

schemes have been proposed for QST using atomic systems [2, 9, 10, 12, 31], trapped ions [3, 11], spin chains [32–34], superconductors [35–38] and nitrogen-vacancy centers [13]. Dissipative dynamics has also been introduced into the QST working in circuit QED [39] and Rydberg atom systems [40]. Very recently, deterministic QESD and QST have been implemented experimentally in a superconducting circuit system [14] using microwave photons based on an all-microwave cavity-assisted Raman process.

The QESD and QST schemes between two remote fiber-connected cavities (nodes) can be roughly categorized into the following cases, as sketched in figure 1. For cases (a, b, c), two separate nodes are operated one by one in sequence or simultaneously, and measurement of the output photons is required. For cases (d, e) with dissipative dynamics involved, the QESD is achieved by a steady state due to competition between the drive and decoherence. But these two cases are not for QST, which works based on unitary dynamics. Case (f) is a new scheme proposed in the present work, which, unlike the previous QESD and QST schemes, has the following favorable characteristics: (i) two qubits employed for QESD and QST are not necessary

---

[3] Author to whom any correspondence should be addressed.
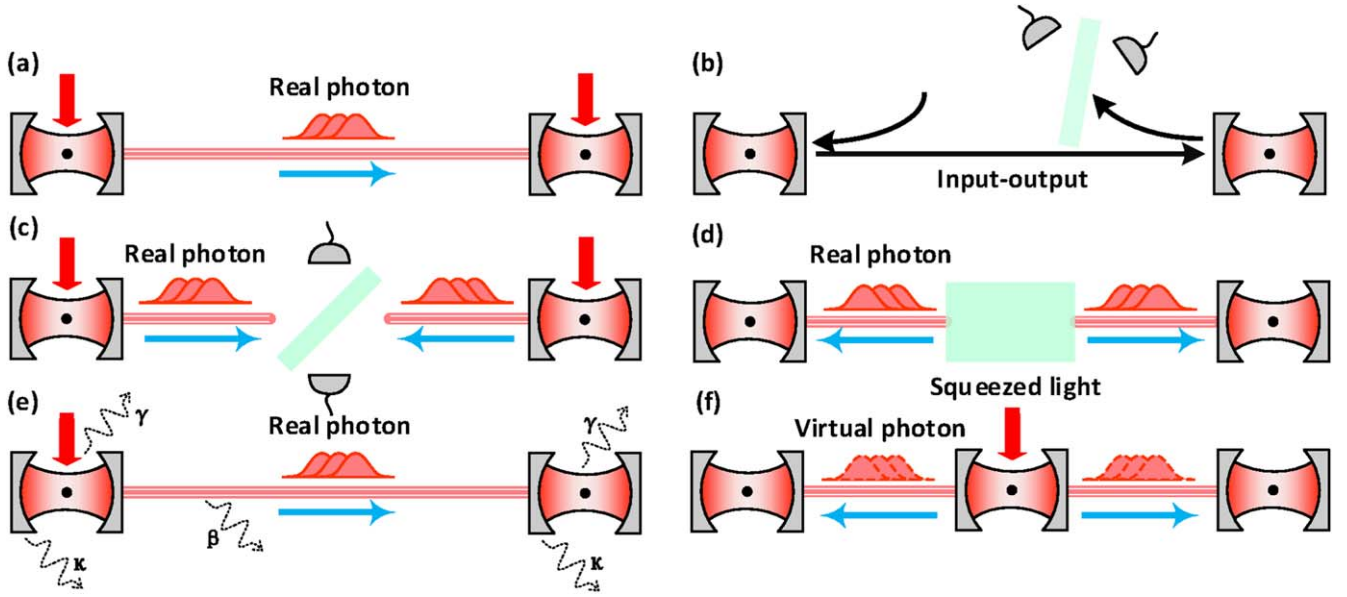
Figure 1. Schematics for typical schemes to create long distance entanglement. (a) The input–output process of photons due to laser-driven atoms. By interacting with the input photons of the laser, the atom emits a photon to the cavity mode in the left node. Then the photon transmits to the right node through an optical fiber and interacts with the laser-driven atom there to complete the QESD and QST [1, 14–16, 21] . (b) Similar to (a) but without laser driving [17–22]. (c) Interference of photons from the atoms in different nodes due to laser driving simultaneously [2, 12]. (d) Involvement of squeezed light under dissipation. Two atoms trapped in different nodes are driven by squeezed light simultaneously and then get entangled in steady states under dissipation [23]. (e) Dissipative dynamics. One or both of the laser-driven atoms in fiber-connected nodes distribute entanglement in a steady state [24, 25]. (f) The present scheme: the quantum entangled state and QST between two atoms in the edge cavities can be achieved conditioned on one-step operation only on the atom in the middle cavity through the virtual photon process. The state of the driving atom (in the middle cavity) is almost invariant while the atoms in the edge cavities are free of laser driving.
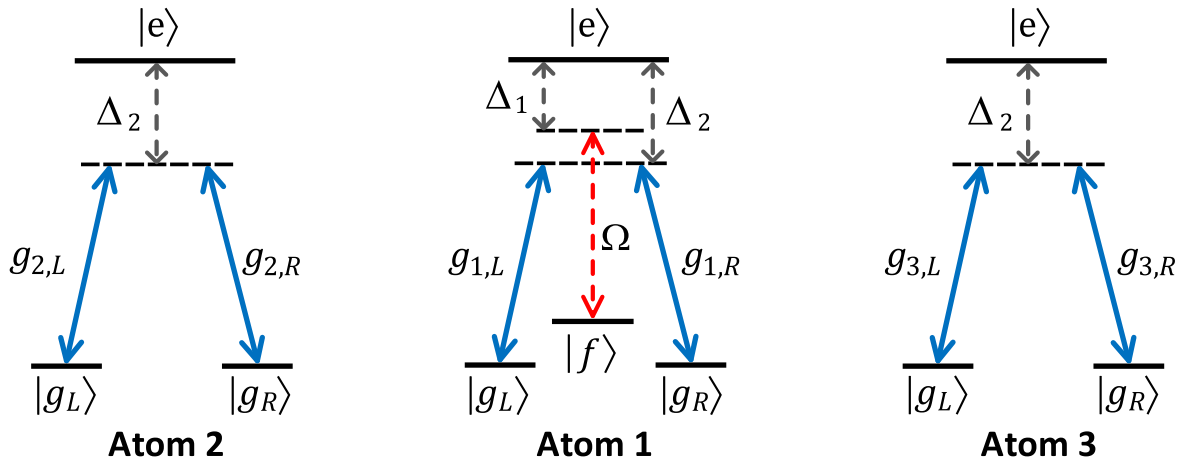
Figure 2. Level scheme for figure 1(f), where the transitions $|e\rangle_n \leftrightarrow |g_{L(R)}\rangle_n$ ($n = 1, 2, 3$ denoting different atoms as labeled at the bottom) are off-resonantly coupled to the left(right)-circularly polarized modes of the cavities. Detunings Δ_2 exist in transitions $|e\rangle_n \leftrightarrow |g_{L(R)}\rangle_n$ and the corresponding coupling constant is $g_{n,L(R)}$. Another laser is applied to off-resonantly drive the transition $|e\rangle_1 \leftrightarrow |f\rangle_1$ in atom 1 with detuning Δ_1 and Rabi frequency Ω.

under actual operations, but are coupled/entangled due to an auxiliary atom and virtually excited photons; (ii) the state of the auxiliary atom remains invariant throughout the scheme, which makes the scheme robust to decoherence. The paper is organized as follows. We first present an effective Hamiltonian for the atom–cavity–fiber model, based on which QESD and QST are implemented. Then we assess how well the scheme can be accomplished and how robust it is against imperfections and dissipation. Experimental feasibility is justified based on labora-tory-available values. The results show that the fidelity of the

system is more than 96.26% by adjusting laser shape. Finally, we give a brief conclusion.

2. The system and Hamiltonians

2.1. The basic model

Our scheme consists of three atoms confined, respectively, in three identical bimodal cavities connected by optical fibers.

Each cavity, as detailed in figure 2, contains a single three-level atom interacting with the cavity by the Jaynes–Cummings model [41] under the rotating-wave approximation [42]. In the interaction picture, the total Hamiltonian can be written, in units of $\hbar = 1$, as

$$
\hat{H}_I = \hat{H}_{CA} + \hat{H}_{LA} + \hat{H}_{CF},
$$
$$
\hat{H}_{CA} = \sum_{k=1}^{3} \sum_{j=L,R} g_{k,j} \hat{a}_{k,j} |e\rangle_k \langle g_j| e^{i\Delta_2 t} + \text{H.c.},
$$
$$
\hat{H}_{LA} = \Omega |e\rangle_1 \langle f| e^{i\Delta_1 t} + \text{H.c.},
$$
$$
\hat{H}_{CF} = \sum_{k=1}^{2} \sum_{j=L,R} \nu \hat{b}_{k,j}^{\dagger} (\hat{a}_{1,j} + \hat{a}_{k+1,j}) + \text{H.c.}, \quad (1)
$$

where $\hat{H}_{CA}$, $\hat{H}_{LA}$ and $\hat{H}_{CF}$ denote the cavity–atom interaction, the laser–atom interaction and the cavity–fiber interaction, respectively. $\hat{a}_{k,j}$ ($k = 1, 2, 3$; $j = L, R$) is the annihilation operator of the j-circularly polarized mode of the cavity k; $\hat{b}_{k,j}$ ($k = 1, 2$) is the annihilation operator of the j-circularly polarized mode of the optical fiber k; ν is the coupling strength between the cavities and the fibers [43, 44]; and $g_{k,j}$ is the coupling strength between the atom k ($k = 1, 2, 3$) and two circularly polarized modes of the cavity k. A laser field is applied to atom 1 with Rabi frequency Ω. Δ_2 and Δ_1 are, respectively, detunings in the transitions $|e\rangle_n \leftrightarrow |g_{L(R)}\rangle_n$ and $|e\rangle_1 \leftrightarrow |f\rangle_1$.

H_{CF} is a working Hamiltonian for high-fineess cavities under resonant operations over timescales much longer than the fiber's round-trip time [43–45] in the short fiber limit. We assume the mode separation between neighboring fiber modes to be $2\pi c/L$. This means that the number of the fiber modes coupling to the cavity mode is of the order of $N = (l\overline{\nu})/(2\pi c)$, where $\overline{\nu}$ is the cavity decay rate under the coupling with the fibers and c is the light speed in optical fibers. In this case, we set $N \leqslant 1$ and the coupling of the cavity mode to an individual fiber mode can be calculated approximately as $\sqrt{4\overline{\nu}\pi c/L}$. As such, there is only one resonant mode $\hat{b}_k$ of the fiber k coupled between the adjacent cavities.

2.2. Effective Hamiltonian

To gain an insight into the significant nature of the system, we first perform the following bosonic-mode transformation [43] for $\hat{H}_I$,

$$
\hat{c}_{\pm\sqrt{3},j} = \frac{1}{2\sqrt{3}} (2\hat{a}_{1,j} + \hat{a}_{2,j} + \hat{a}_{3,j} \pm \sqrt{3}\hat{b}_{1,j} \pm \sqrt{3}\hat{b}_{2,j}),
$$
$$
\hat{c}_{\pm,j} = \frac{1}{2} (-\hat{a}_{2,j} + \hat{a}_{3,j} \mp \hat{b}_{1,j} \pm \hat{b}_{2,j}),
$$
$$
\hat{c}_0 = \frac{1}{\sqrt{3}} (-\hat{a}_{1,j} + \hat{a}_{2,j} + \hat{a}_{3,j}), \quad (2)
$$

which rewrites $\hat{H}_I$ as $\hat{H}_I' = \hat{H}_{AC}' + \hat{H}_{LA}' + \hat{H}_{CF}'$ with

$$
\hat{H}_{AC}' = \sum_{j=L,R} \frac{g_{1,j}}{\sqrt{3}} (\hat{c}_{+\sqrt{3},j} + \hat{c}_{-\sqrt{3},j} - \hat{c}_{0,j})
$$
$$
\times |e\rangle_1 \langle g_j| e^{i\Delta_2 t} + \sum_{k=2}^{3} \sum_{j=L,R} \frac{g_{k,j}}{2\sqrt{3}}
$$
$$
\times [\hat{c}_{+\sqrt{3},j} + \hat{c}_{-\sqrt{3},j} + (-1)^{k-1}\sqrt{3}\hat{c}_{+,j}
$$
$$
+ (-1)^{k-1}\sqrt{3}\hat{c}_{-,j} + 2\hat{c}_{0,j}]
$$
$$
\times |e\rangle_k \langle g_j| e^{i\Delta_2 t} + \text{H.c.},
$$
$$
\hat{H}_{LA}' = \Omega |e\rangle_1 \langle f| e^{i\Delta_1 t} + \text{H.c.},
$$
$$
\hat{H}_{CF}' = \nu \sum_{j=L,R} (\sqrt{3}\hat{c}_{+\sqrt{3},j}^{\dagger}\hat{c}_{+\sqrt{3},j}
$$
$$
- \sqrt{3}\hat{c}_{-\sqrt{3},j}^{\dagger}\hat{c}_{-\sqrt{3},j} + \hat{c}_{+,j}^{\dagger}\hat{c}_{+,j} - \hat{c}_{-,j}^{\dagger}\hat{c}_{-,j}). \quad (3)
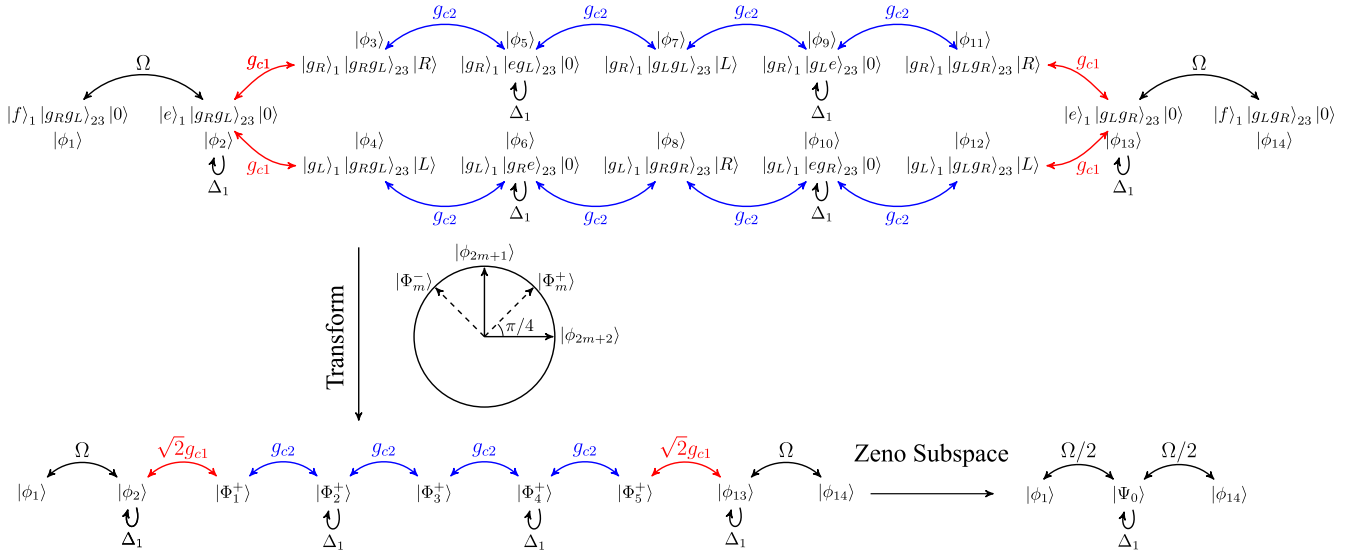$$

Then turning it into the interaction representation by performing the unitary operation $e^{-i(\hat{H}_{CF}' - \Delta_1 \sum_{k=1}^{3} |e\rangle_k \langle e|)t}$, we obtain $\hat{H}_I'' = \hat{H}_{AC}'' + \hat{H}_{LA}''$ where

$$
\hat{H}_{AC}'' = \sum_{j=L,R} \frac{g_{1,j}}{\sqrt{3}} (\hat{c}_{+\sqrt{3},j} e^{i\delta_{+\sqrt{3}}t}
$$
$$
+ \hat{c}_{-\sqrt{3},j} e^{i\delta_{-\sqrt{3}}t} - \hat{c}_{0,j} e^{i\delta_0 t}) |e\rangle_1 \langle g_j|
$$
$$
+ \sum_{k=2}^{3} \sum_{j=L,R} \frac{g_{k,j}}{2\sqrt{3}} [\hat{c}_{+\sqrt{3},j} e^{i\delta_{+\sqrt{3}}t} + \hat{c}_{-\sqrt{3},j} e^{i\delta_{-\sqrt{3}}t}
$$
$$
+ (-1)^{k-1}\sqrt{3}\hat{c}_{+,j} e^{i\delta_+ t}
$$
$$
+ (-1)^{k-1}\sqrt{3}\hat{c}_{-,j} e^{i\delta_- t} + 2\hat{c}_{0,j} e^{i\delta_0 t}] \times |e\rangle_k \langle g_j| + \text{H.c.}
$$
$$
(4)
$$

and $\hat{H}_{LA}'' = \Delta_1 \sum_{j=1}^{3} |e\rangle_j \langle e| + \Omega (|e\rangle_1 \langle f| + |f\rangle_1 \langle e|)$ with the detuning satisfying $\delta_n = \Delta_2 - \Delta_1 + n\nu$ ($n = \pm\sqrt{3}, \pm, 0$).

By selecting suitable detuning $\delta_m = 0$, in the large detuning limit $\delta_n \gg g_{k,j} (n \neq m)$, equation (4) can be reduced to a simple model in which a bimodal cavity $c_{n,j}$ is coupled to an imaginary five-level atom system. All in all, the large detuning limit corresponds to $\nu \gg g_{k,j}$. Choosing $\delta_+ = 0$ ($\delta_- = 0$), under the rotating-wave approximation only the terms containing $\hat{c}_{+,j}$ ($\hat{c}_{-,j}$) in equation (4) are reserved. However these two modes $\hat{c}_{+,j}$ ($\hat{c}_{-,j}$) are decoupled with state $|e\rangle_1$ which implies that atom 1 is out of interaction with the bimodal field. Similarly, if $\delta_n = 0$ ($n = \pm\sqrt{3}, 0$) there are also only two modes $\hat{c}_{n,j}$. However, the state $|e\rangle_1$ is coupled to these two modes and a full coupling structure is obtained. In these situations, we write the effective Hamiltonians in a uniform form ($n = \pm\sqrt{3}, 0$),

$$
\hat{H}_{eff} = \Delta_1 \sum_{k=1}^{3} |e\rangle_k \langle e| + \left[\Omega |e\rangle_1 \langle f| \right.
$$
$$
\left. + \sum_{j=L,R} \bar{g}_j \hat{c}_{n,j} |\vartheta\rangle_j \langle g_j| + \text{H.c.} \right] \quad (5)
$$

Figure 3. Schematic for the simplification steps of Hamiltonians from equation (6) to equation (8) and then to equation (11).

where we define the state $|\vartheta\rangle_j := \sum_{k=1}^{3} \bar{g}_{k,j}|e\rangle_k / \bar{g}_j$ with the normalization coefficient $\bar{g}_j$, $\bar{g}_{1,j} = g_{1,j}/\sqrt{3}$ and $\bar{g}_{k,j} = g_{k,j}/2\sqrt{3}$ with $k = 2, 3$. (Some details can be seen in the appendix.) Equation (5) is one of the main results in our model. To simplify the representation, we set $\bar{g}_{1,j} = g_{c1}$ and $\bar{g}_{k,j} = g_{c2}$ with $k = 2, 3$.

3. Simplification in a subspace

For our purpose of achieving high-quality QESD and QST, we encode qubits in the ground states $|g_L g_R\rangle_{23}$ and $|g_R g_L\rangle_{23}$. To this end, we impose the system to be initially in the state $|\phi_0\rangle = |f\rangle_1 |g_R g_L\rangle_{23}|000\rangle_c|00\rangle_f$ denoting atoms 1, 2 and 3 in the states $|f\rangle$, $|g_R\rangle$ and $|g_L\rangle$, respectively, and the fibers and three cavities in vacuum states. This initial state, after the bosonic-mode transformation in equation (2), becomes $|\phi_0\rangle \rightarrow |\phi_1\rangle = |f\rangle_1 |g_R g_L\rangle_{23}|0\rangle$, as the initial state of the effective Hamiltonian described by equation (5). $|0\rangle$ in $|\phi_1\rangle$ is the vacuum state of the bosonic mode in equation (5). In order to describe $\hat{H}_{eff}$ in single-exciton space, we introduce new basis states $\{|\phi_n\rangle\}$, as given in the appendix, and rewrite equation (5) as

$$\begin{aligned}
\hat{\mathcal{H}}_I &= \hat{\mathcal{H}}_g + \hat{\mathcal{H}}_\Omega + \hat{\mathcal{H}}_\Delta, \\
\hat{\mathcal{H}}_g &= g_{c1}(|\phi_2\rangle\langle\phi_3| + |\phi_{13}\rangle\langle\phi_{11}| \\
&\quad + |\phi_2\rangle\langle\phi_4| + |\phi_{13}\rangle\langle\phi_{12}|) \\
&\quad + g_{c2}(|\phi_5\rangle\langle\phi_3| + |\phi_8\rangle\langle\phi_{10}|) \\
&\quad + g_{c2}(|\phi_5\rangle\langle\phi_7| + |\phi_{12}\rangle\langle\phi_{10}|) \\
&\quad + g_{c2}(|\phi_6\rangle\langle\phi_8| + |\phi_9\rangle\langle\phi_{11}|) \\
&\quad + g_{c2}(|\phi_6\rangle\langle\phi_4| + |\phi_9\rangle\langle\phi_7|) + \text{H.c.}, \\
\hat{\mathcal{H}}_\Omega &= \Omega(|\phi_2\rangle\langle\phi_1| + |\phi_{13}\rangle\langle\phi_{14}|) + \text{H.c.}, \\
\hat{\mathcal{H}}_\Delta &= \Delta_1(|\phi_2\rangle\langle\phi_2| + |\phi_5\rangle\langle\phi_5| + |\phi_6\rangle\langle\phi_6| \\
&\quad + |\phi_9\rangle\langle\phi_9| + |\phi_{10}\rangle\langle\phi_{10}| + |\phi_{13}\rangle\langle\phi_{13}|).
\end{aligned} \quad (6)$$

Equation (6) can be graphically understood as shown in figure 3. Because two paths exist in the coupling from $|\phi_2\rangle$ to $|\phi_{13}\rangle$, we further consider a group of transformations,

$$|\Phi_m^\pm\rangle = \frac{1}{\sqrt{2}}(|\phi_{2m+1}\rangle \pm |\phi_{2m+2}\rangle), \quad (m = 1, 2, ..., 5) \quad (7)$$

and then, by setting $\sqrt{2} g_{c1} = g_{c2} = g$, equation (6) becomes

$$\begin{aligned}
\hat{\mathcal{H}}_I &= \hat{\mathcal{H}}_g + \hat{\mathcal{H}}_\Omega + \hat{\mathcal{H}}_\Delta, \\
\hat{\mathcal{H}}_g &= g(|\phi_2\rangle\langle\Phi_1^+| + |\Phi_5^+\rangle\langle\phi_{13}|) \\
&\quad + g \sum_{m=1}^{4} \sum_{n=\pm} |\Phi_m^n\rangle\langle\Phi_{m+1}^n| + \text{H.c.}, \\
\hat{\mathcal{H}}_\Omega &= \Omega(|\phi_1\rangle\langle\phi_2| + |\phi_{13}\rangle\langle\phi_{14}|) + \text{H.c.}, \\
\hat{\mathcal{H}}_\Delta &= \Delta_1\Bigg[|\phi_2\rangle\langle\phi_2| + |\phi_{13}\rangle\langle\phi_{13}| \\
&\quad + \sum_{n=\pm} (|\Phi_2^n\rangle\langle\Phi_2^n| + |\Phi_4^n\rangle\langle\Phi_4^n|)\Bigg],
\end{aligned} \quad (8)$$

which implies that the system is effectively divided into two subspaces relating to $\{|\Phi_m^+\rangle\}$ and $\{|\Phi_m^-\rangle\}$ (see figure 3). If the system is initially prepared in $|\phi_1\rangle$ or $|\phi_{14}\rangle$, no state would evolve into the subspace regarding $\{|\Phi_m^-\rangle\}$. As such, in the following treatment, we just consider the state evolution within a nine-dimensional Hilbert subspace spanned by $\{|\phi_1\rangle, |\phi_2\rangle, |\phi_{13}\rangle, |\phi_{14}\rangle, |\Phi_1^+\rangle, |\Phi_2^+\rangle, |\Phi_3^+\rangle, |\Phi_4^+\rangle, |\Phi_5^+\rangle\}$.

3.1. Zeno subspace

In this section, we introduce Zeno conditions $\hat{\mathcal{H}}_g \gg \hat{\mathcal{H}}_\Omega$, which means $g \gg \Omega$, to simplify the dynamics of the system. After discarding the subspace regarding $\{|\Phi_m^-\rangle\}$, we rewrite the Hamiltonian equation (8) based on $|\phi_1\rangle$, $|\phi_{14}\rangle$ and the

Table 1. Eigenvalues and eigenstates of $\hat{\mathcal{H}}_g$. Here we define $\xi_{\pm} = \sqrt{2 \pm \sqrt{2}}$ and $\eta_{\pm} = 1 \pm \sqrt{2}$.

Eigenvalues	Eigenstates
$\lambda = 0$	$|\Psi_0\rangle = \frac{1}{2}(|\phi_2\rangle - |\Phi_2^+\rangle + |\Phi_4^+\rangle - |\phi_{13}\rangle)$
$\lambda_1^{\pm} = \pm\sqrt{2}\,g$	$|\Psi_1^{\pm}\rangle = \frac{1}{2\sqrt{2}}(|\phi_2\rangle \pm \sqrt{2}|\Phi_1^+\rangle + |\Phi_2^+\rangle - |\Phi_4^+\rangle \mp \sqrt{2}|\Phi_5^+\rangle - |\phi_{13}\rangle)$
$\lambda_2^{\pm} = \pm g\xi_+$	$|\Psi_2^{\pm}\rangle = \frac{\sqrt{2}}{4\xi_+}[|\phi_2\rangle \pm \xi_+(|\Phi_1^+\rangle + \sqrt{2}|\Phi_2^+\rangle + |\Phi_5^+\rangle) + \eta_+(|\Phi_2^+\rangle + |\Phi_4^+\rangle) + |\phi_{13}\rangle]$
$\lambda_3^{\pm} = \pm g\xi_-$	$|\Psi_3^{\pm}\rangle = \frac{\sqrt{2}}{4\xi_-}[|\phi_2\rangle \pm \xi_-(|\Phi_1^+\rangle - \sqrt{2}|\Phi_2^+\rangle + |\Phi_5^+\rangle) + \eta_-(|\Phi_2^+\rangle + |\Phi_4^+\rangle) + |\phi_{13}\rangle]$

eigenstates of $\hat{\mathcal{H}}_g$(listed in table 1),

$$\hat{\mathcal{H}}_I' = \hat{\mathcal{H}}_g' + \hat{\mathcal{H}}_\Omega' + \hat{\mathcal{H}}_\Delta',$$

$$\hat{\mathcal{H}}_g' = \sum_{m=1}^{3}\sum_{n=\pm} \lambda_m^n |\Psi_m^n\rangle\langle\Psi_m^n|,$$

$$\hat{\mathcal{H}}_\Omega' = \frac{\Omega}{2}[|\Psi_0\rangle + \frac{1}{\sqrt{2}}(|\Psi_1^+\rangle + |\Psi_1^-\rangle)](\langle\phi_1| - \langle\phi_{14}|)$$

$$+ \frac{\Omega}{4}(|\phi_1\rangle + |\phi_{14}\rangle)[\xi_-(\langle\Psi_2^+| + \langle\Psi_2^-|)$$

$$+ \xi_+(\langle\Psi_3^+| + \langle\Psi_3^-|)] + \text{H.c.},$$

$$\hat{\mathcal{H}}_\Delta' = \Delta_1|\Psi_0\rangle\langle\Psi_0| + \frac{\Delta_1}{2}\sum_{m=1}^{3}(|\Psi_m^+\rangle + |\Psi_m^-\rangle)(\langle\Psi_m^+| + \langle\Psi_m^-|). \quad (9)$$

Equation (9) can be further simplified under a unitary transformation $e^{-i\hat{\mathcal{H}}_g't}$ and the condition of quantum Zeno dynamics [46], i.e. omitting the highly oscillating terms for $g \gg \Omega$. Then we have a new simplified Hamiltonian as below,

$$\hat{\mathcal{H}}_{eff} = \frac{\Omega}{2}[|\Psi_0\rangle(\langle\phi_1| - \langle\phi_{14}|)] + \Delta_1|\Psi_0\rangle\langle\Psi_0|$$

$$+ \frac{\Delta_1}{2}\sum_{m=1}^{3}|\Psi_m^{\pm}\rangle\langle\Psi_m^{\pm}|$$

$$+ \frac{\Delta_1}{2}\sum_{m=1}^{3}(e^{i(\lambda_m^+ - \lambda_m^-)t}|\Psi_m^+\rangle\langle\Psi_m^-| + \text{H.c.}. \quad (10)$$

Despite the $|\Psi_m^+\rangle$ and $|\Psi_m^-\rangle$ which are decoupled from $\{|\Psi_0\rangle, |\phi_1\rangle, |\phi_{14}\rangle\}$, the system can be described as a Λ-type three-level quantum system possessing an upper state $|\Psi_0\rangle$ and two lower states $|\phi_1\rangle$ and $|\phi_{14}\rangle$.

3.2. Effective model

Starting from equation (10), for the large detuning condition $\Delta_1 \gg \Omega$, $\hat{\mathcal{H}}_{eff}$ could be further simplified as

$$\hat{\mathcal{H}}_{eff} = \frac{\Omega^2}{4\Delta_1}|\phi_1\rangle\langle\phi_{14}| + \text{H.c.}, \quad (11)$$

which evolves from the initial state $|\phi_1\rangle$ to

$$|\psi(t)\rangle = |f\rangle_1 \otimes \left[\cos\frac{\Omega^2 t}{4\Delta_1}|g_R g_L\rangle_{23}\right.$$

$$\left. - i\sin\frac{\Omega^2 t}{4\Delta_1}|g_L g_R\rangle_{23}\right] \otimes |0\rangle. \quad (12)$$

The evolution on the Hilbert space corresponding to the original Hamiltonian equation (1) is

$$|\psi(t)\rangle = |f\rangle_1 \otimes \left[\cos\frac{\Omega^2 t}{4\Delta_1}|g_R g_L\rangle_{23}\right.$$

$$\left. - i\sin\frac{\Omega^2 t}{4\Delta_1}|g_L g_R\rangle_{23}\right] \otimes |000\rangle_c|00\rangle_f. \quad (13)$$

4. Application

4.1. QESD

Now from the effective Hamiltonian $\hat{\mathcal{H}}_{eff}$ in equation (10) with the initial state $|\phi_0\rangle$, we tune Δ_1 and Ω, and the system evolves to

$$|\psi(t)\rangle = |f\rangle_1 \otimes [\cos\omega t|g_R g_L\rangle_{23}$$

$$- i\sin\omega t|g_L g_R\rangle_{23}] \otimes |000\rangle_c|00\rangle_f, \quad (14)$$

where ω is $\Omega^2/4\Delta_1$. The result clearly shows that throughout the evolution, atom 1 stays in the state $|f\rangle_1$ and the bosonic mode remains in a vacuum state, whereas atom 2 and atom 3 become entangled. The maximum entanglement occurs at $\tau = \pi/4\omega$ yielding the target state $|\psi_{tar}\rangle = \frac{1}{\sqrt{2}}|f\rangle_1 \otimes (|g_R g_L\rangle_{23} - i|g_L g_R\rangle_{23}) \otimes |000\rangle_c|00\rangle_f$. If we have a $\pi/2$-phase operation on atom 2, the system will be a standard Bell state $|Bell\rangle = \frac{1}{\sqrt{2}}|f\rangle_1 \otimes (|g_R g_L\rangle_{23} + |g_L g_R\rangle_{23}) \otimes |000\rangle_c|00\rangle_f$.

4.2. QST

Based on equation (13), we may achieve the QST for arbitrary quantum states. For example, for an initial quantum state

$$|\psi_0\rangle = |f\rangle_1 \otimes [\alpha|g_R\rangle_2 + \beta|g_L\rangle_2] \otimes |g_L\rangle_3 \otimes |000\rangle_c|00\rangle_f, \quad (15)$$
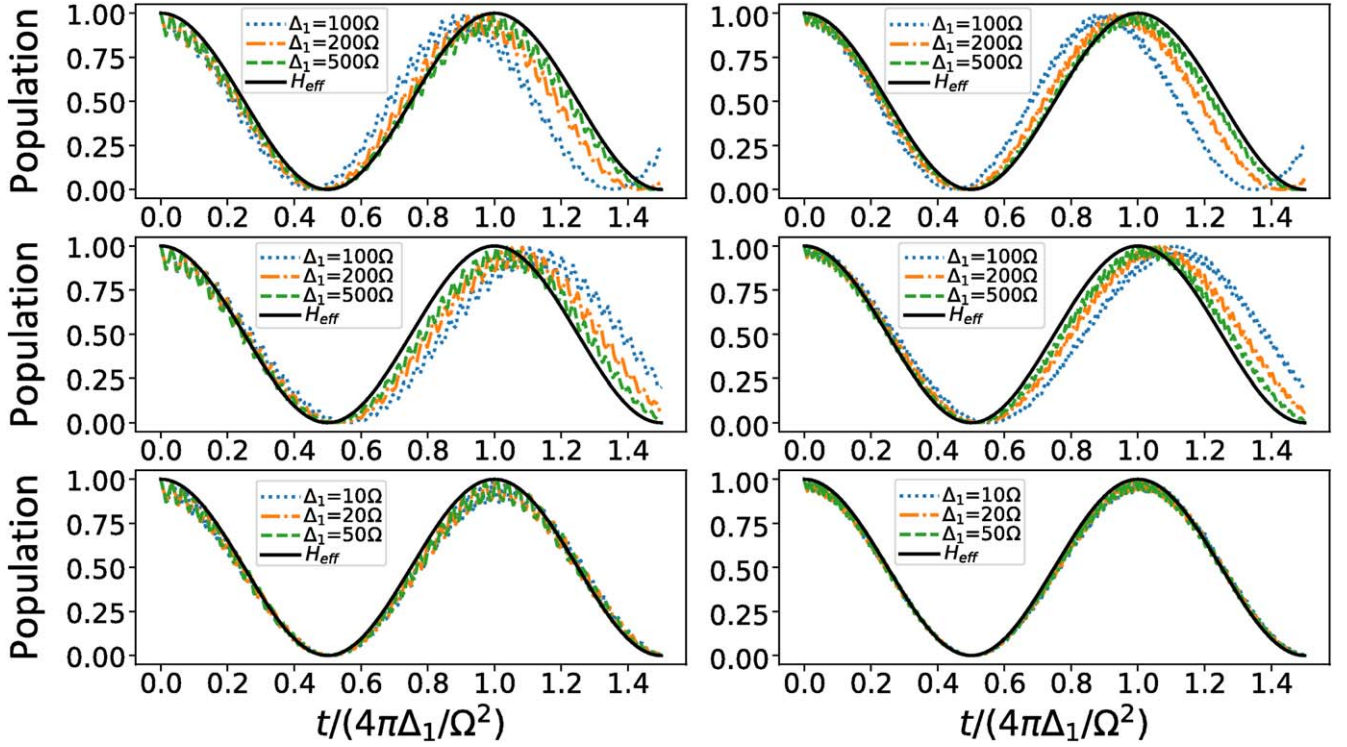
an evolution for $\omega t = \pi/2$ and then a $\pi/2$-phase operation on atom 3 could yield the state transfer from atom 2 to atom 3 as

$$|\psi_{QST}\rangle = |f\rangle_1 \otimes |g_L\rangle_2 \otimes [\alpha|g_R\rangle_3 + \beta|g_L\rangle_3] \otimes |000\rangle_c|00\rangle_f. \quad (16)$$

5. Numerical simulation

Since we have simplified the original Hamiltonian by a series of approximations, we have to justify the effective Hamiltonian

J. Phys. B: At. Mol. Opt. Phys. **53** (2020) 035503

J-X Liu *et al*

Figure 4. Comparison of the population of $|\phi_0\rangle$ from the original Hamiltonian with that from the effective Hamiltonian. (a1) $\nu = 5g = 25\Omega$ and (b1) $\nu = 5\sqrt{2}\,g = 50\Omega$, where other parameters used are $\Delta_2 = \Delta_1 - \sqrt{3}\,\nu$, $g_{c1} = \sqrt{6}\,g/2$ and $g_{c2} = 2\sqrt{3}\,g$. (a2)$\nu = 5g = 25\omega$ and (b2)$\nu = 5\sqrt{2}\,g = 50\Omega$, where other parameters used are $\Delta_2 = \Delta_1 + \sqrt{3}\,\nu$, $g_{c1} = \sqrt{6}\,g/2$ and $g_{c2} = 2\sqrt{3}\,g$. (a3)$\nu = 5g = 25\omega$ and (b3)$\nu = 5\sqrt{2}\,g = 50\,\Omega$, where other parameters used are $\Delta_1 = \Delta_2$, $g_{c1} = -\sqrt{6}\,g/2$ and $g_{c2} = \sqrt{3}\,g$.

after simplification. In order to make the simplified model hold, the relationships that need to be satisfied are $\nu \gg g \gg \Omega$ and $\Delta_1 \gg \Omega$. Here we exemplify the QESD and check numerically the validity of those approximations by comparing the original Hamiltonian with the effective one.

5.1. Different parameter conditions

In this subsection, we check three groups of parameter conditions, $\delta_{+\sqrt{3}}$, $\delta_{-\sqrt{3}}$, δ_0, by comparing the results of the time evolution of $|\phi_0\rangle$ calculated from the original and the effective Hamiltonians (see equation (10)).

(i) $\delta_{+\sqrt{3}} = 0$

In this situation, the parameter relationship that needs to be satisfied is $\Delta_1 - \Delta_2 = \sqrt{3}\,\nu \gg g \gg \Omega$ and $\Delta_1 \gg \Omega$. As plotted in figures 4(a1), (b1), Δ_1 mainly decides the frequency of the evolution while g and ν influence the local fluctuation. This situation needs a large Δ which means a long operation time $\tau = \pi\Delta/\Omega^2$.

(ii) $\delta_{-\sqrt{3}} = 0$

Nearly the same as (i); the parameter relationship that needs to be satisfied is $\Delta_2 - \Delta_1 = \sqrt{3}\,\nu \gg g \gg \Omega$ and $\Delta_1 \gg \Omega$. As plotted in figures 4(a2), (b2), the result is very similar to (i). That is the reason why the calculation of (ii) is similar to (i).

(iii) $\delta_0 = 0$

In this situation, ν is independent from Δ_1 and Δ_2. The parameter relationship that needs to be satisfied is $\nu \gg g \gg \Omega$ and $\Delta_1 \gg \Omega$. As plotted in figures 4(a3), (b3), when $\Delta_1 = \Delta_2$, the results of the effective model and the actual model match very well.

From the fitting in figure 4, we know that the frequency of the evolution in our scheme is mainly controlled by detuning Δ_1 and Δ_2. Meanwhile, local fluctuation is caused by hopping strength ν and coupling strength g. In consideration of the impact of operation time, we adopt the scheme in (iii) for further discussion.

The fidelity of the system is calculated by

$$F = \langle \psi_{tar} | \hat{\rho}(\tau) | \psi_{tar} \rangle \qquad (17)$$

where $|\psi_{tar}\rangle$ is the target state that we want to implement, and $\hat{\rho}(\tau)$ denotes the density operator of this system at operation time τ. Then, we check the validity of the quantum Zeno condition $g \gg \Omega$ and hopping strength ν. The result in figure 5(a) reveals that g mainly affects the fidelity of the system. When $g \geqslant 20\,\Omega$, the effective model also has a high fidelity when the condition $\nu \gg g$ is not fully satisfied.

A sufficiently large ν can suppress the excitation of boson modes except $\hat{c}_{0,j}$. Experimentally, it is relatively difficult to achieve high-strength fiber–cavity coupling ν. In a cold atom system, the coupling between microcavity and fiber is about 20 MHz, which is not strong enough to satisfy our
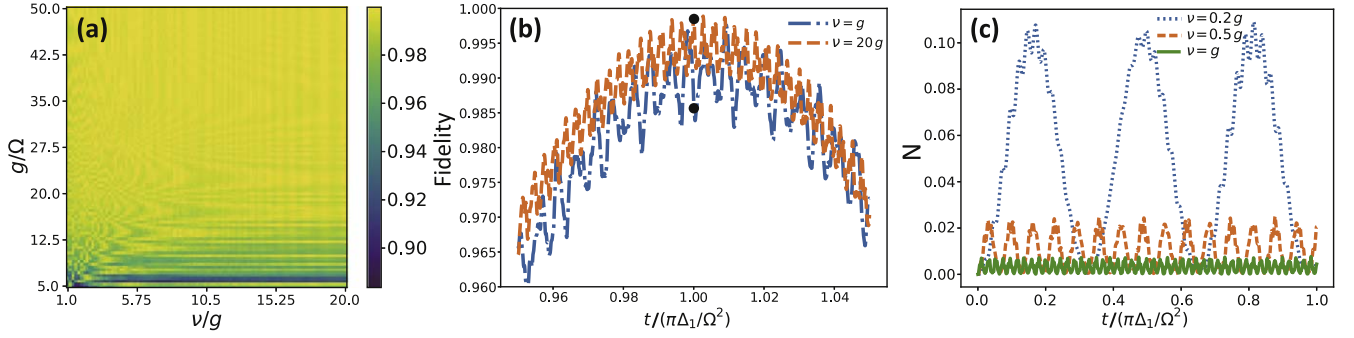
Figure 5. (a) F of the original Hamiltonian with respect to g and ν at $\tau = \pi\Delta_1/\Omega^2$, where $\Delta_1 = \Delta_2 = 20\Omega$, $g_{c1} = -\sqrt{6}\,g/2$ and $g_{c2} = \sqrt{3}\,g$. (b) The effect on local evolution fluctuation due to different ν when $g = 20\,\Omega$. (c) The total population of photons in mode $\hat{c}_{\pm,L(R)}$.
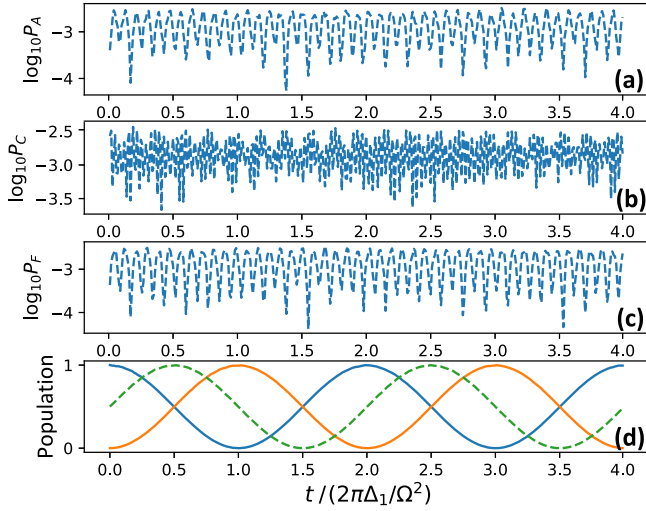
Figure 6. Dynamics of the system, where (a) $\log_{10}(P_A)$ with P_A being the sum of all the atomic excited-state populations; (b) $\log_{10}(P_C)$ with P_C being the sum of the populations of the cavity's nonzero photon-number states; (c) $\log_{10}(P_F)$ with P_F being the sum of the populations of the fiber's nonzero photon-number states; (d) population in $|g_R g_L\rangle$ (blue solid), $|g_L g_R\rangle$ (brown solid) and F (green dashed), which is the fidelity of creating the target state $|\psi_{tar}\rangle$. Parameters used here: $g = 30\,\Omega$, $g_{c1} = -\sqrt{6}\,g/2$, $g_{c2} = \sqrt{3}\,g$, $\nu = 50\,\Omega$, $\Delta_1 = \Delta_2 = 20\,\Omega$.

Figure 7. Fidelity of the target state at $\tau = \pi\Delta_1/\Omega^2$ under different values of dissipation. Parameters used here: $g = 30\,\Omega$, $g_{c1} = -\sqrt{6}\,g/2$, $g_{c2} = \sqrt{3}\,g$, $\nu = 50\,\Omega$, $\Delta_1 = \Delta_2 = 20\,\Omega$.
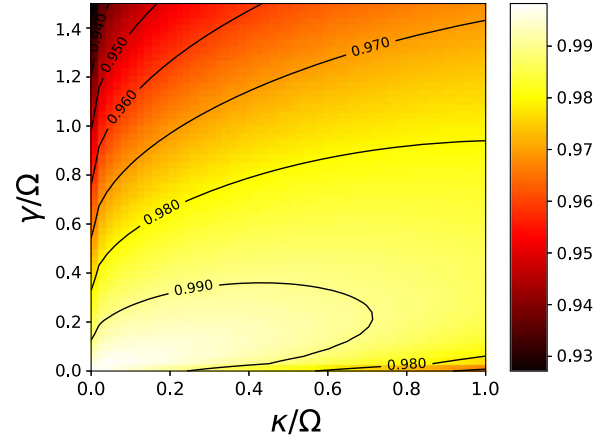
condition $\nu \gg g_{k,j}$ [47]. The fluctuation of fidelity will increase but the maximal value of the fidelity is almost invariant when ν takes a small value, as shown in figure 5(b). The population of modes $\hat{c}_{\pm,j}$ is the main reason for the failure of our scheme. Furthermore, we find when $\nu \lesssim g_{k,j}$, the total population N of mode $\hat{c}_{\pm,L(R)}$ is an oscillation curve in figure 5(c) where

$$N = \hat{c}_{+,L}^{\dagger}\hat{c}_{+,L} + \hat{c}_{+,R}^{\dagger}\hat{c}_{+,R} + \hat{c}_{-,L}^{\dagger}\hat{c}_{-,L} + \hat{c}_{-,R}^{\dagger}\hat{c}_{-,R} \quad (18)$$

and N could be a small number at some time which means there are few photons escaping the boson mode that we use to transfer. This will lead to a displacement of the frequency we predict but the effective model still stands.

5.2. Validity of the virtual photon

One of the advantages of our scheme is the achievement of entanglement and state transfer between the distant nodes via
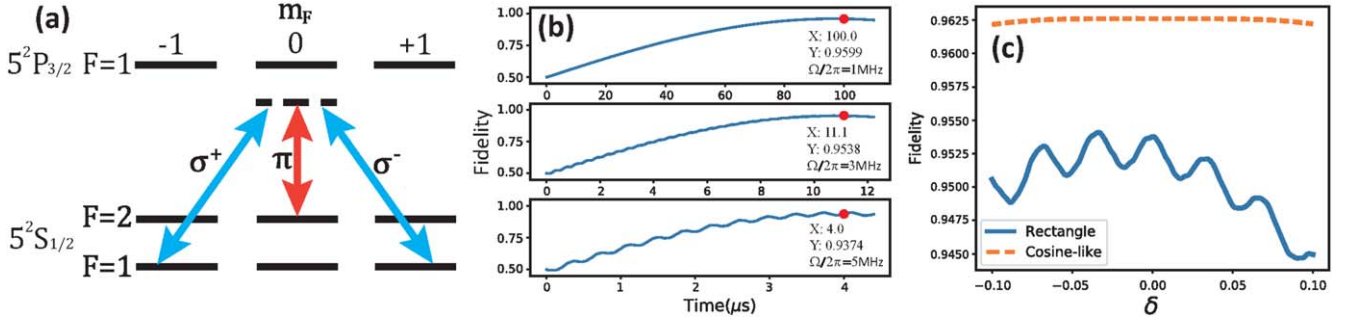
virtual photon effects. As presented in figure 6, we justify this virtual photon condition numerically, in which the approximation can be found to work nearly perfectly. The population in excited states, cavities and fibers are all less than 0.01 and this illustrates that the system is robust. In the next section, we will discuss the robustness of the system in detail.

5.3. Robustness against decoherence

Taking decoherence into consideration, we check the evolution of the whole system using the Lindblad master equation,

$$\dot{\rho} = i[\rho, \hat{H}_I] + \frac{1}{2}\sum_{k=1}^{3}\sum_{j=L,R}[2\mathcal{L}_{k,j}\rho\mathcal{L}_{k,j}^{\dagger}$$

$$- (\mathcal{L}_{k,j}\mathcal{L}_{k,j}^{\dagger}\rho + \rho\mathcal{L}_{k,j}^{\dagger}\mathcal{L}_{k,j})]$$

$$+ \frac{1}{2}\sum_{m=1}^{3}\sum_{j=L,R}[2\mathcal{L}_{m,j}\rho\mathcal{L}_{m,j}^{\dagger} - (\mathcal{L}_{m,j}\mathcal{L}_{m,j}^{\dagger}\rho + \rho\mathcal{L}_{m,j}^{\dagger}\mathcal{L}_{m,j})]$$

$$+ \frac{1}{2}\sum_{n=1}^{2}\sum_{j=L,R}[2\mathcal{L}_{n,j}\rho\mathcal{L}_{n,j}^{\dagger} - (\mathcal{L}_{n,j}\mathcal{L}_{n,j}^{\dagger}\rho + \rho\mathcal{L}_{n,j}^{\dagger}\mathcal{L}_{n,j})]$$

$$+ \frac{1}{2}[2\mathcal{L}_0\rho\mathcal{L}_0^{\dagger} - (\mathcal{L}_0\mathcal{L}_0^{\dagger}\rho + \rho\mathcal{L}_0^{\dagger}\mathcal{L}_0)],$$

$$(19)$$

Figure 8. (a) Energy levels and related transitions in ^{87}Rb atoms, where σ^+, σ^- and π denote the left-circular, right-circular and linear polarizations, respectively. (b) Time evolution of the fidelity for creating the target state with different values of Ω, where $g_{n,j}/2\pi = 100$ MHz, $\gamma/2\pi = 6$ MHz, $\kappa_c/2\pi = 1.5$ MHz, $\kappa_f/2\pi = 152$ kHz, $\nu/2\pi = 20$ MHz and $\Delta_1(\Delta_2)/2\pi = 200$ MHz. *X* and *Y*, respectively, denote the operation time and fidelity at the red point. (c) Fidelity with respect to the deviation from the ideal operation time.

where $\mathcal{L}_0 = \sqrt{\gamma_1}|f\rangle_1\langle e|$, $\mathcal{L}_{k,j} = \sqrt{\gamma_{k,j}}|g_j\rangle_k\langle e|$, $\mathcal{L}_{m,j} = \sqrt{\kappa_{m,j}}\hat{a}_m$ and $\mathcal{L}_{n,j} = \sqrt{\kappa_{n,j}}\hat{b}_n$ describe various decoherence effects in the system. To simplify our treatment, we assume $\gamma_1 = \gamma_{1,j} = \gamma/3$, $\gamma_{2,j} = \gamma_{3,j} = \gamma/2$ and $\kappa_{m,j} = \kappa_{n,j} = \kappa/2$ with the spontaneous emission rate γ of each atom and the photon leakage rate κ of the cavity or fiber.

We plot in figure 7 the fidelity, with respect to the ideal case, as a function of γ/Ω and κ/Ω at evolving time $t = \pi\Delta_1/\Omega^2$. This scheme is very robust against decoherence induced by atomic spontaneous emissions and photonic leakages from the cavity–fiber system. From figure 7, we can see that when γ and κ are around 1.5Ω and Ω respectively, the fidelity at t can still exceed 0.93 even if $\nu \gg g$ is not satisfied. The atomic spontaneous emissions rate γ influences the system more than other decaying factors.

6. Experimental feasibility

The system under consideration could be realized in cold alkali-metal atoms, such as ^{135}Cs or ^{87}Rb [48–50], as considered in figure 8(a). Based on recent experimental reports employing high-Q cavities and strong atom–cavity coupling [51–56], we may choose the parameters as $g_{n,j}/2\pi \sim 100$ MHz, $\gamma/2\pi \sim 6$ MHz and $\kappa_c/2\pi \sim 1.5$ MHz. The fiber decay rate and coupling strength can be set as $\kappa_f/2\pi \sim 152$ kHz [57] and $\nu/2\pi = 20$ MHz [47].

Using these parameters, we simulate our scheme with different values of Ω, as shown in figure 8(b), where the fidelity is about 95.38% after the system has evolved for 11.1 μs under $\Omega/2\pi = 3$ MHz.

Actually, the system is mainly affected by the decay of atom γ. Moreover, coupling of the fiber and cavity is limited by the technique. Experimentally, there are two ways to improve the fidelity of our model. (1) Suppressing spontaneous emission. People have developed techniques such as adding two parallel conducting planes or mirrors around atoms [58, 59], trapping them in a microwave cavity [60] to eliminate the vacuum modes at the transition frequency. (2) Improving coupling strength. Fibers can be replaced by

current-biased Josephson junctions. Correspondingly, the cavity QED system can be replaced by a circuit QED system [61] and the coupling could achieve $g/2\pi \approx 183$ MHz [62]. Maybe this is a promising system.

In order to minimize the influence of experimental imperfections, we try to accelerate the implementation as discussed above. From equation (10) we know the final fidelity depending on $\int \Omega^2 dt$. As such, we choose a cosine-like function,

$$\Omega(t) = \Omega_m\left[\cos\left(\frac{2\pi t}{T'} - \pi\right) + 1\right]/2, \qquad (20)$$

where Ω_m is the maximum amplitude. To satisfy $\int_0^{T'} \Omega(t)^2 dt = \int_0^T \Omega^2 dt$, we obtain $3\Omega_m^2 T' = 8\Omega^2 T$, implying that a larger Ω_m could effectively accelerate entanglement generation and QST. Figure 8(c) indicates that the laser pulse with cosine-like function works much better than the usual rectangular form with fidelity 96.26%.

7. Conclusion

To summarize, we have proposed a practical scheme to achieve QESD and QST in an atom–cavity–fiber model, which could work for future quantum networks. Three favorable features, i.e. the auxiliary atom under laser driving is always in the ground state, no excitation for every atom and field mode throughout implementation, and no actual operation performed on the atoms for entanglement, make our scheme experimentally feasible with current laboratory techniques and robust to experimental imperfections. In this context, we argue that our scheme is easily extended to the multi-atom case with each cavity confining N atoms, for which the coupling strength could become larger with more atoms involved and thus less operation time is required. We argue that our scheme would be helpful for exploiting quantum networks connected by optical fibers or even in a wireless way. Finally, we suggest the choice of $\Delta_1 = \Delta_2$, under which the laser action time can be decreased greatly and ν is independent of Δ_1 and Δ_2. In addition, the value of ν can take $\nu \lesssim g$ when $g \gg \Omega$.

Acknowledgments

Appendix

Choosing different detuning δ_n we could reduce equation (4) to the following effective Hamiltonians,

(i) $\delta_{+\sqrt{3}} = 0$

$$\hat{H}_{eff1} = \left[\Omega |e\rangle_1 \langle f| + \sum_{j=L,R} \left(\frac{g_{1,j}}{\sqrt{3}} \hat{c}_{+\sqrt{3},j} |e\rangle_1 \langle g_j| \right. \right.$$
$$\left. \left. + \sum_{k=2}^{3} \frac{g_{k,j}}{2\sqrt{3}} \hat{c}_{+\sqrt{3},j} |e\rangle_k \langle g_j| \right) + \text{H.c.} \right] + \Delta_1 \sum_{j=1}^{3} |e\rangle_j \langle e|, \quad (A.1)$$

where $\delta_{-\sqrt{3}}$, δ_+, δ_-, $\delta_0 \gg g$. In the large detuning limit, we have conditions $(\sqrt{3}+1)\nu \gg g$, $(\sqrt{3}-1)\nu \gg g$ and $\sqrt{3}\nu \gg g$.

(ii) $\delta_{-\sqrt{3}} = 0$

$$\hat{H}_{eff2} = \left[\Omega |e\rangle_1 \langle f| + \sum_{j=L,R} \left(\frac{g_{1,j}}{\sqrt{3}} \hat{c}_{-\sqrt{3},j} |e\rangle_1 \langle g_j| \right. \right.$$
$$\left. \left. + \sum_{k=2}^{3} \frac{g_{k,j}}{2\sqrt{3}} \hat{c}_{-\sqrt{3},j} |e\rangle_k \langle g_j| \right) + \text{H.c.} \right] + \Delta_1 \sum_{j=1}^{3} |e\rangle_j \langle e|, \quad (A.2)$$

where $\delta_{+\sqrt{3}}$, δ_+, δ_-, $\delta_0 \gg g$. In the large detuning limit, we have conditions $(\sqrt{3}+1)\nu \gg g$, $(\sqrt{3}-1)\nu \gg g$ and $\sqrt{3}\nu \gg g$.

(iii) $\delta_0 = 0$

$$\hat{H}_{eff3} = \left[\Omega |e\rangle_1 \langle f| + \sum_{j=L,R} \left(-\frac{g_{1,j}}{\sqrt{3}} \hat{c}_{0,j} |e\rangle_1 \langle g_j| \right. \right.$$
$$\left. \left. + \sum_{k=2}^{3} \frac{g_{k,j}}{\sqrt{3}} \hat{c}_{0,j} |e\rangle_k \langle g_j| \right) + \text{H.c.} \right] + \Delta_1 \sum_{j=1}^{3} |e\rangle_j \langle e|, \quad (A.3)$$

where $\delta_{-\sqrt{3}}$, $\delta_{+\sqrt{3}}$, δ_+, δ_-, $\gg g$. In the large detuning limit, we have conditions $\sqrt{3}\nu \gg g$ and $\nu \gg g$.

(iv) $\delta_+ = 0$

$$\hat{H}_{eff4} = \left[\Omega |e\rangle_1 \langle f| + \sum_{k=2}^{3} \frac{g_{k,j}}{2} \hat{c}_{+,j} |e\rangle_k \langle g_j| \right)$$
$$+ \text{H.c.} \right] + \Delta_1 \sum_{j=1}^{3} |e\rangle_j \langle e|, \quad (A.4)$$

where $\delta_{+\sqrt{3}}$, $\delta_{-\sqrt{3}}$, δ_0, $\delta_- \gg g$. In the large detuning limit, we have conditions $(\sqrt{3}+1)\nu \gg g$, $(\sqrt{3}-1)\nu \gg g$ and $\nu \gg g$.

(v) $\delta_- = 0$

$$\hat{H}_{eff5} = \left[\Omega |e\rangle_1 \langle f| + \sum_{k=2}^{3} \frac{g_{k,j}}{2} \hat{c}_{-,j} |e\rangle_k \langle g_j| \right)$$
$$+ \text{H.c.} \right] + \Delta_1 \sum_{j=1}^{3} |e\rangle_j \langle e|, \quad (A.5)$$

where $\delta_{+\sqrt{3}}$, $\delta_{-\sqrt{3}}$, δ_0, $\delta_+ \gg g$. In the large detuning limit, we have conditions $(\sqrt{3}+1)\nu \gg g$, $(\sqrt{3}-1)\nu \gg g$ and $\nu \gg g$.

So to summarize, $\nu \gg g$ should be satisfied in equation (5).

In order to describe $\hat{H}_{eff}$ in a single-exciton space, we introduce a set of bases as below,

$$|\phi_1\rangle = |f\rangle_1 |g_R g_L\rangle_{23} |0\rangle, \quad |\phi_2\rangle = |e\rangle_1 |g_R g_L\rangle_{23} |0\rangle,$$
$$|\phi_3\rangle = |g_R\rangle_1 |g_R g_L\rangle_{23} |R\rangle, \quad |\phi_4\rangle = |g_L\rangle_1 |g_R g_L\rangle_{23} |L\rangle,$$
$$|\phi_5\rangle = |g_R\rangle_1 |e g_L\rangle_{23} |0\rangle, \quad |\phi_6\rangle = |g_L\rangle_1 |g_R e\rangle_{23} |0\rangle,$$
$$|\phi_7\rangle = |g_R\rangle_1 |g_L g_L\rangle_{23} |L\rangle, \quad |\phi_8\rangle = |g_L\rangle_1 |g_R g_R\rangle_{23} |R\rangle,$$
$$|\phi_9\rangle = |g_R\rangle_1 |g_L e\rangle_{23} |0\rangle, \quad |\phi_{10}\rangle = |g_L\rangle_1 |e g_R\rangle_{23} |0\rangle,$$
$$|\phi_{11}\rangle = |g_R\rangle_1 |g_L g_R\rangle_{23} |R\rangle, \quad |\phi_{12}\rangle = |g_L\rangle_1 |g_L g_R\rangle_{23} |L\rangle,$$
$$|\phi_{13}\rangle = |e\rangle_1 |g_L g_R\rangle_{23} |0\rangle, \quad |\phi_{14}\rangle = |f\rangle_1 |g_L g_R\rangle_{23} |0\rangle. \quad (A.6)$$

Then we reach equation (6) in the main text.

ORCID iDs

Shi-Lei Su ⓘ https://orcid.org/0000-0002-2153-5827

References

[1] Cirac J I, Zoller P, Kimble H J and Mabuchi H 1997 *Phys. Rev. Lett.* **78** 3221–4
[2] Duan L M and Kimble H J 2003 *Phys. Rev. Lett.* **90** 253601
[3] Browne D E, Plenio M B and Huelga S F 2003 *Phys. Rev. Lett.* **91** 067901
[4] Ekert A K 1991 *Phys. Rev. Lett.* **67** 661–3
[5] Briegel H J, Dür W, Cirac J I and Zoller P 1998 *Phys. Rev. Lett.* **81** 5932–5
[6] Cleve R, Gottesman D and Lo H K 1999 *Phys. Rev. Lett.* **83** 648–51
[7] Bennett C H, Brassard G, Crépeau C, Jozsa R, Peres A and Wootters W K 1993 *Phys. Rev. Lett.* **70** 1895–9
[8] Cirac J I, Ekert A K, Huelga S F and Macchiavello C 1999 *Phys. Rev. A* **59** 4249–54
[9] Bose S, Knight P L, Plenio M B and Vedral V 1999 *Phys. Rev. Lett.* **83** 5158–61
[10] Feng X L, Zhang Z M, Li X D, Gong S Q and Xu Z Z 2003 *Phys. Rev. Lett.* **90** 217902
[11] Simon C and Irvine W T M 2003 *Phys. Rev. Lett.* **91** 110405
[12] Duan L M, Lukin M, Cirac J I and Zoller P 2001 *Nature* **414** 413

J. Phys. B: At. Mol. Opt. Phys. **53** (2020) 035503

J-X Liu *et al*

[13] Childress L, Taylor J M, Sørensen A S and Lukin M D 2006 *Phys. Rev. Lett.* **96** 070504

[14] Kurpiers P *et al* 2018 *Nature* **558** 264–7

[15] Clark S, Peng A, Gu M and Parkins S 2003 *Phys. Rev. Lett.* **91** 177901

[16] Pyrkov A N and Byrnes T 2013 *New J. Phys.* **15** 093019

[17] Duan L M and Kimble H J 2004 *Phys. Rev. Lett.* **92** 127902

[18] Duan L M, Wang B and Kimble H J 2005 *Phys. Rev. A* **72** 032333

[19] Hacker B, Welte S, Rempe G and Ritter S 2016 *Nature* **536** 193

[20] Tiecke T, Thompson J D, de Leon N P, Liu L, Vuletić V and Lukin M D 2014 *Nature* **508** 241

[21] Kimble H J 2008 *Nature* **453** 1023

[22] Song J, Xia Y and Song H S 2008 *Phys. Rev. A* **78** 024302

[23] Kraus B and Cirac J I 2004 *Phys. Rev. Lett.* **92** 013602

[24] Shen L T, Chen R X, Yang Z B, Wu H Z and Zheng S B 2014 *Opt. Lett.* **39** 6046–9

[25] Jin Z, Su S L, Zhu A D, Wang H F and Zhang S 2017 *Opt. Express* **25** 88–101

[26] Wang Q, Tan M Y, Liu Y and Zeng H S 2009 *J. Phys. B: At. Mol. Opt. Phys.* **42** 125503

[27] Sheng Y B and Deng F G 2010 *Phys. Rev. A* **81** 042332

[28] Yin J *et al* 2012 *Nature* **488** 185

[29] Brask J B, Jiang L, Gorshkov A V, Vuletic V, Sørensen A and Lukin M D 2010 *Phys. Rev. A* **81** 020303

[30] Mabuchi H and Doherty A C 2002 *Science* **298** 1372–7

[31] Matsukevich D and Kuzmich A 2004 *Science* **306** 663–6

[32] Bose S 2003 *Phys. Rev. Lett.* **91** 207901

[33] Christandl M, Datta N, Ekert A and Landahl A J 2004 *Phys. Rev. Lett.* **92** 187902

[34] Yao N Y, Jiang L, Gorshkov A V, Gong Z X, Zhai A, Duan L M and Lukin M D 2011 *Phys. Rev. Lett.* **106** 040505

[35] Sillanpää M A, Park J I and Simmonds R W 2007 *Nature* **449** 438

[36] Majer J *et al* 2007 *Nature* **449** 443

[37] Mei F, Chen G, Tian L, Zhu S L and Jia S 2018 *Phys. Rev. A* **98** 012331

[38] Xiang Z L, Zhang M, Jiang L and Rabl P 2017 *Phys. Rev. X* **7** 011035

[39] Wang C and Gertler J M 2018 (arXiv:1809.03571)

[40] Li D X and Shao X Q 2019 *Phys. Rev. A* **99** 032348

[41] Jaynes E 1963 *Proc. IEEE* **51** 89

[42] Shore B W 1993 *J. Mod. Opt.* **40** 1195

[43] Serafini A, Mancini S and Bose S 2006 *Phys. Rev. Lett.* **96** 010503

[44] Pellizzari T 1997 *Phys. Rev. Lett.* **79** 5242

[45] Van Enk S, Kimble H, Cirac J and Zoller P 1999 *Phys. Rev. A* **59** 2659

[46] Facchi P and Pascazio S 2002 *Phys. Rev. Lett.* **89** 080401

[47] Wu X W, Zou C L, Cui J M, Yang Y, Han Z F and Guo G C 2009 *J. Phys. B: At. Mol. Opt. Phys.* **42** 085401

[48] Wilk T, Webster S C, Kuhn A and Rempe G 2007 *Science* **317** 488–90

[49] Lettner M, Mücke M, Riedl S, Vo C, Hahn C, Baur S, Bochmann J, Ritter S, Dürr S and Rempe G 2011 *Phys. Rev. Lett.* **106** 210503

[50] Steck D A 2019 Alkali D Line Data (http://steck.us/alkalidata)

[51] Spillane S, Kippenberg T, Painter O and Vahala K 2003 *Phys. Rev. Lett.* **91** 043902

[52] Vernooy D, Ilchenko V S, Mabuchi H, Streed E and Kimble H 1998 *Opt. Lett.* **23** 247–9

[53] Armani D, Kippenberg T, Spillane S and Vahala K 2003 *Nature* **421** 925

[54] Buck J and Kimble H 2003 *Phys. Rev. A* **67** 033806

[55] Spillane S, Kippenberg T, Vahala K, Goh K, Wilcut E and Kimble H 2005 *Phys. Rev. A* **71** 013817

[56] Barclay P 2006 *Appl. Phys. Lett.* **89** 131108

[57] Gordon K J, Fernandez V, Townsend P D and Buller G S 2004 *IEEE J. Quantum Electron.* **40** 900–8

[58] Jhe W, Anderson A, Hinds E, Meschede D, Moi L and Haroche S 1987 *Phys. Rev. Lett.* **58** 666

[59] Hulet R G, Hilfer E S and Kleppner D 1985 *Phys. Rev. Lett.* **55** 2137

[60] Gabrielse G and Dehmelt H 1985 *Phys. Rev. Lett.* **55** 67

[61] Zhang F Y, Liu B, Chen Z H, Wu S L and Song H S 2014 *Ann. Phys.* **346** 103–12

[62] DiCarlo L *et al* 2009 *Nature* **460** 240

[63] Johansson J, Nation P and Nori F 2012 *Comput. Phys. Commun.* **183** 1760–72